Seasonality of Surface Chlorophyll in the Red Sea

by

Mohammed Elamin Basir Hassan Ahmed

A thesis submitted in partial fulfillment for the
degree of Master of Science

Faculty of Mathematics and Natural Sciences
Geophysical Institute

October 2012

To my parents

UNIVERSITY OF BERGEN

Abstract

Faculty of Mathematics and Natural Sciences
Geophysical Institute

Master of Science

by

Mohammed Elamin Basir Hassan Ahmed

Although the understanding of the oceanography of the Red Sea has been developed over the last few decades, but we still have a little knowledge about the influences of the physical factors on the phytoplankton activity. The purpose of the present study was initially to quantify and investigate the seasonal variation of surface chlorophyll concentration (CHL-a) at three zones in the Red Sea (north, middle and south). The second goal is to identify the controlling factors which seem to have an effect on the phytoplankton bloom during the same period of the study. To reach our goals, we use remote sensing data (surface chlorophyll, sea surface temperature and photosynthetically available radiation), oceanographic data (wind speed), and modeling data (mixed layer depth) received during the period 1998–2009. The data are analyzed using BEAM/VISAT software and statistical methods to reveal principle features of the phytoplankton bloom. The results indicate different mechanisms of the phytoplankton bloom and different importance of controlling factors at the three zones of the Red Sea.

Acknowledgements

This thesis would not have been possible without the support of numerous individuals and institutions. I would like to convey my heartfelt gratitude to my supervisor, Dr. Anton Korosov, for his constant guidance, advice and helpful discussion. I am sincerely and heartily grateful to my co-supervisor, Dr. Abdirahman Omar, also many thanks go to Dr. Ingunn Skjelvan who gave me help and good advices.

I would like to thank the NOMA program, which is financed by the Norwegian Agency for Development (NORAD) for providing the fund for my study. Also many thanks for the Geophysical Institute in university of Bergen. I offer my regards and blessings to the program coordinator Dr. Knut Barthel for his continuous support, excellent guidance, caring, and patience.

I am truly indebted and thankful to Dr. Mohammed Ali Alfaki for his patience and continuous support from the initial to the final level of the master. I owe my deepest gratitude to Elfatih Bakry for his greatest support, and advice. Also many thanks to Dr. Al-fatih Ali for helping and support. I would like to thanks all the members of the Institute of Marine Research, and College of Marine Science in the Red Sea University, who they have contributed immensely to my personal and professional time at Port Sudan. Many thanks to my colleagues and my best friends through their encouragement and support to do this work.

Great thanks to my parents, Bashir Hassan Ahmed and Saadia Madani AbdulMajed, who have always given me the strength and wisdom to be sincere in my work, for setting high moral standards and supporting me through their hard work, and for their unselfish love and affection. This thesis is dedicated to them and to my aunt, Almutaz Madani AbdulMajed who has been my friend, guide and philosopher. Also I dedicate this thesis to my brothers and my sisters who have always helped me and believed that I could do it. This thesis is dedicated to them. This thesis is dedicated to my aunt, Almutaz Madani AbdulMajed who has been my friend, guide and philosopher, to my brothers, sisters and my best friends who they always helped me and believed that I could do it.

Contents

Chapter 1

Introduction

Phytoplankton biomass is an important bio-physical characteristic that is commonly used to appraise the clarity and color of the sea water. The photosynthetic pigment chlorophyll-a (CHL-a) is the most widely used measure of phytoplankton biomass (Moses et al., 2009). The main reason CHL-a being used to indicate the availability of phytoplankton biomass is because it is the most common pigment in most of marine phytoplankton (Li et al., 2002). Thus, the water quality can be monitored by the estimation of CHL-a concentration near the surface water (Moses et al., 2009).

The food chain in the ocean begins with organisms that are able to utilize light energy to synthesize organic matter from inorganic chemicals (photosynthesis). The oceanic photosynthesis is carried out by unicellular plants known as phytoplankton (Sarmiento and Gruber, 2006). Throughout the photosynthesis process, phytoplankton uses its associated pigment (CHL-a pigments) to capture the energy from the sunlight. Phytoplankton use this energy to acquire the dissolved carbon dioxide from the sea water, convert it into organic compounds (carbohydrates), and release oxygen (Alvain et al., 2010). When the light permeate to the ocean surface layer, phytoplankton pigments (CHL-a) selectively absorbs blue and red wavelengths and scatters the green ones. As the density of phytoplankton biomass increases, more blue light will absorbed and more green light will scatters that's why the color of the ocean shift from blue to green (Alvain et al., 2010).

Phytoplankton bloom is a rapid accumulation of phytoplankton biomass in water column. It occurs when the rate of cell growth significantly exceed the rate of cell loss, and there are some factors controlling this process in the ocean. Controlling factor (or limiting factor) is defined as "the best available substance that supports the maximum yields relative to the requirement of the biomass synthesis" (Liebig and Playfair, 1845). Light, nutrients, and temperature are the most important

factors that controlling the abundance and the growth rate of phytoplankton. While the grazing by zooplankton and sinking are the factors that controlling the loss rate of phytoplankton (Cloern, 2001; Sarmiento and Gruber, 2006). Briefly occurrence of any of the growth factors with the absence of grazers can be the adventitious event in bloom initiation (Mackey et al., 2009).

Generally phytoplankton need light and nutrients for growth, the light come from above (sun light) and the nutrients come from below (deep water), these are the main factors which control the phytoplankton production in the ocean (Mann and Lazier, 2006). Nutrients are not distributed evenly in the water column, they are high in the deep water and depleted in the surface due to the uptake by phytoplankton (Mann and Lazier, 2006). Mixed layer depth is an important factor to bring nutrients to the surface, especially in tropical and oligotrophic water. On seasonal time scales, and at subtropical latitudes, stronger winds and the decrease in sea surface temperature are the factors which deepen the mixed layer during winter, while the increase in temperature acts to stratify the water column and result in shallower mixed layer (Sarmiento et al., 2004). In oligotrophic waters, the mixed layer depth is a useful indicator of biological production because its maximum depth determines the depth from which deep nutrient-rich waters can be combined to the surface to refill nutrient supplies exhausted by biological activity in the photic zone (Sarmiento et al., 2004).

The understanding of the Red Sea oceanography has been developed over the last few decades, but still the information related to the biological processes in the water column is limited. Particularly, we still have poor understanding of how phytoplankton abundance varies during the seasons, how phytoplankton accumulations are distributed through different regions, and what are the factors that control the seasonal variation in the Red Sea.

This short knowledge is due to several reasons: The existing literature that describes these processes is limited, and the limited availability of suitable data due to the restrictions imposed by the political situations in the countries surrounding the Red Sea. Thus, the majority of the previous studies have been based on satellite data (Acker et al., 2008).

In the present work, we used satellite ocean color data (surface chlorophyll concentration (CHL-a), sea surface temperature (SST) and photosynthetically available radiation (PAR)), modeling data (mixed layer depth (MLD)) and oceanographic data (wind speed (U)).

The goal of the this study is to:

- Quantify (CHL-a) and investigate seasonal variations using satellite data at three zones in the Red Sea (North, Middle, and Southern zone).

- Identify controlling factors, the seasonal variations of the physical factors (SST, PAR, MLD, and U) and their impact on (CHL-a) and phytoplankton bloom. This is due to the fact that, the biological processes cannot be understood in isolation because the physical processes create the conditions of many biological processes and also influences the rates of them (Mann and Lazier, 2006).

Chapter 2

Red Sea Oceanography

2.1 Location of the Red Sea

The Red Sea is an elongated and narrow tropical marginal sea separating northern Africa from the Arabian subcontinent, extending from (12.5°N) to about (30°N), over a distance of about 2250 km with an average width of 280 km (Acker et al., 2008). It terminates to the North to Gulf of Suez which is connected to the Suez channel and the Gulf of Aqaba (Eliat). Suez channel represent the connection between the Red Sea and Mediterranean Sea. At the southern end, Red Sea has a

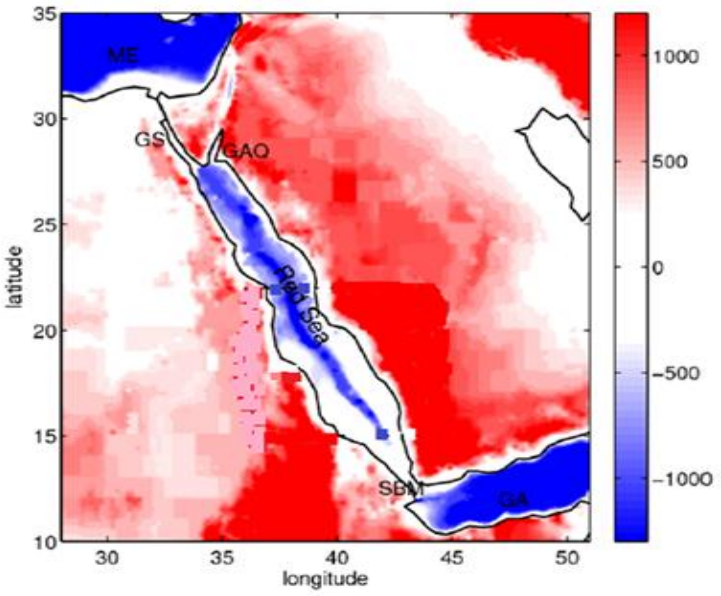

FIGURE 2.1: A Red Sea topographic map. The colors are the elevation of the topography (unit: m). The locations of Gulf of Aqaba (GAQ), Gulf of Suez (GS), Gulf of Aden (GA), Mediterranean Sea (ME), and Strait of Bab el Mandeb (SBM) are shown. This figure is from (Zhai, 2011).

minimum width of about 25km at the straits of Bab el Mandeb where the exchange

between the Red sea and the Indian Ocean takes place, and there is a shallow sill with a greatest depth of about 137 m – Hanish Sill located slightly north of Bab el Mandeb (Zhai, 2011). When the Arabian seawater enters the Red Sea through the Bab el Mandeb strait, it become saltier as it goes northwards due to the lake of permanent rivers and poor rainfall (Lindell and Post, 1995). Figure 2.1 illustrates the topographic map of the Red Sea.

2.2 Physical Processes

2.2.1 Surface winds in the Red Sea

Red Sea is surrounded by an arid land; desert and semi-desert region, the existence of the high mountains on the both sides of the entire Red Sea have the greatest influences on the surface winds. These mountains may control the direction of the winds to blow parallel to the longitudinal axis of the Red Sea (Jiang et al., 2009). The variable wind driven monsoon currents which are result of the Indian monsoon seasonally influences the Red Sea. There are two wind seasons in the

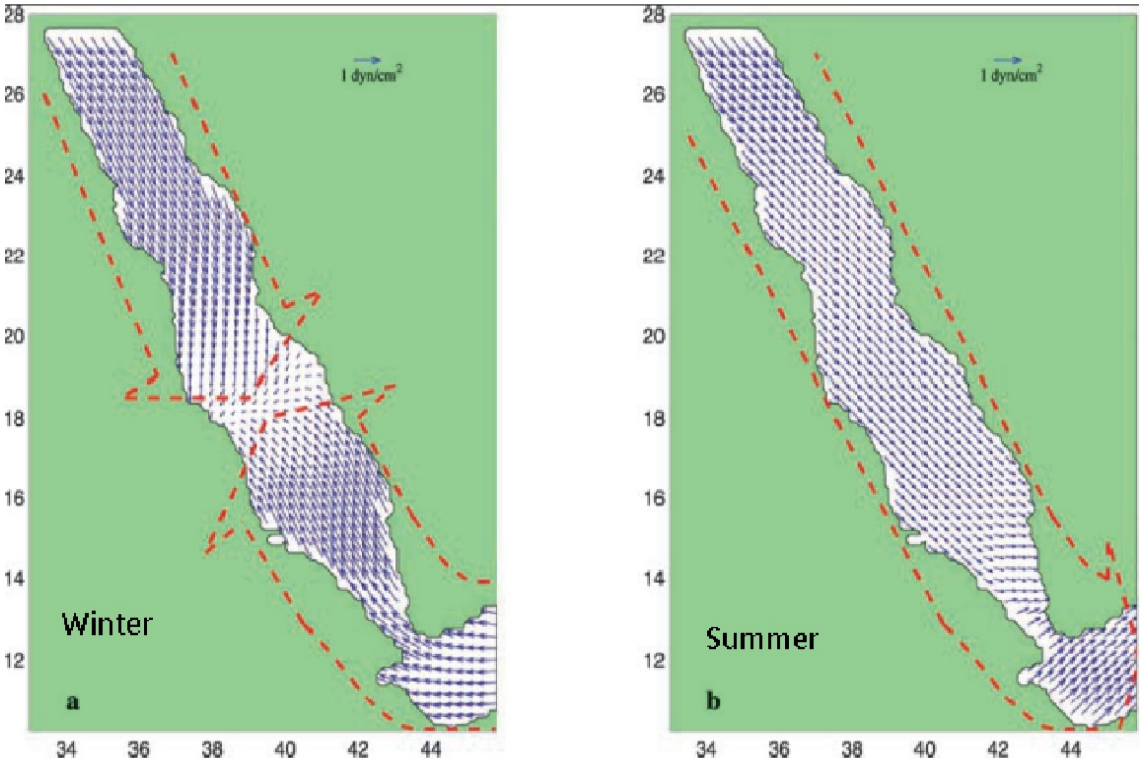

FIGURE 2.2: Wind-stress fields during winter (a) and summer season (b) from COADS climatology (Sofianos and Johns, 2002).

Red Sea, the summer season (southwest monsoon, May to September) when north to northwest winds are blowing along the total axis of the Red Sea, the winter

season (northeast monsoon, October to April) when south to southeast winds are blowing over the southern part of the Red Sea (Morcos, 1970). These two monsoon seasons are reverse to each other because during the summer, surface waters are heaped up along the African coast and some upwelling occurs along the Arabian coast while during winter, surface waters are heaped up on the Arabian coast and upwelling occurs on the African coast (Morcos, 1970). The Indian monsoon system is controlling the direction of winds in the southern zone of the Red Sea to blow from southeast during winter to northwest during summer (Pedgley, 1974). The eastern Mediterranean weather systems are controlling the direction of winds in the northern zone of the Red Sea to blow from the northwest all the year (Sofianos and Johns, 2002). In the central zone there is a very weak wind speed and the wind field is convergent and results in sinking of surface water (Morcos, 1970; Sofianos and Johns, 2002). Figure 2.1 (a and b) illustrate the winter and summer wind stress field throughout the Red Sea.

2.2.2 Temperature and Salinity

Air temperature and Sea Surface Temperature (SST) in the Red Sea increase from north to south, get their maximum values in the southern zone, and there is a linear relationship between them. One of the hottest climate regions in the world is located south of 18°N and the shore of the Gulf of Aden (Morcos, 1970).

During summer, the surface water temperature increases towards the south and get its maximum value (≈32°C) at about 14°N, then it decreases towards the Strait of Bab el Mandeb due to the inflow of the Gulf Of Aden Water (Morcos, 1970). SST distribution in the southern Red Sea is markedly influenced by the wind direction induced by the monsoon (Edwards and Head, 1987). During winter the water with high sea surface temperature move northward until it reaches 19°N (Patzert, 1974).

The central zone is classified as the region of a maximum temperature, which decreases towards the northern and southern ends of the Red Sea. This is due to a very weak wind speed at this zone where the wind is convergent throughout the year (Morcos, 1970; Sofianos and Johns, 2002). The seasonal change in the position of the central zone is controlling by the monsoons. During winter the winds blow from both ends of the Red Sea towards the central zone (zone of maximum temperature), while in summer north-westerly winds dominate the whole area throughout the year. There is a thermocline which is weaker in winter than in summer, it's stronger below the central zone than the northern and southern zone of the Red Sea (Morcos, 1970).

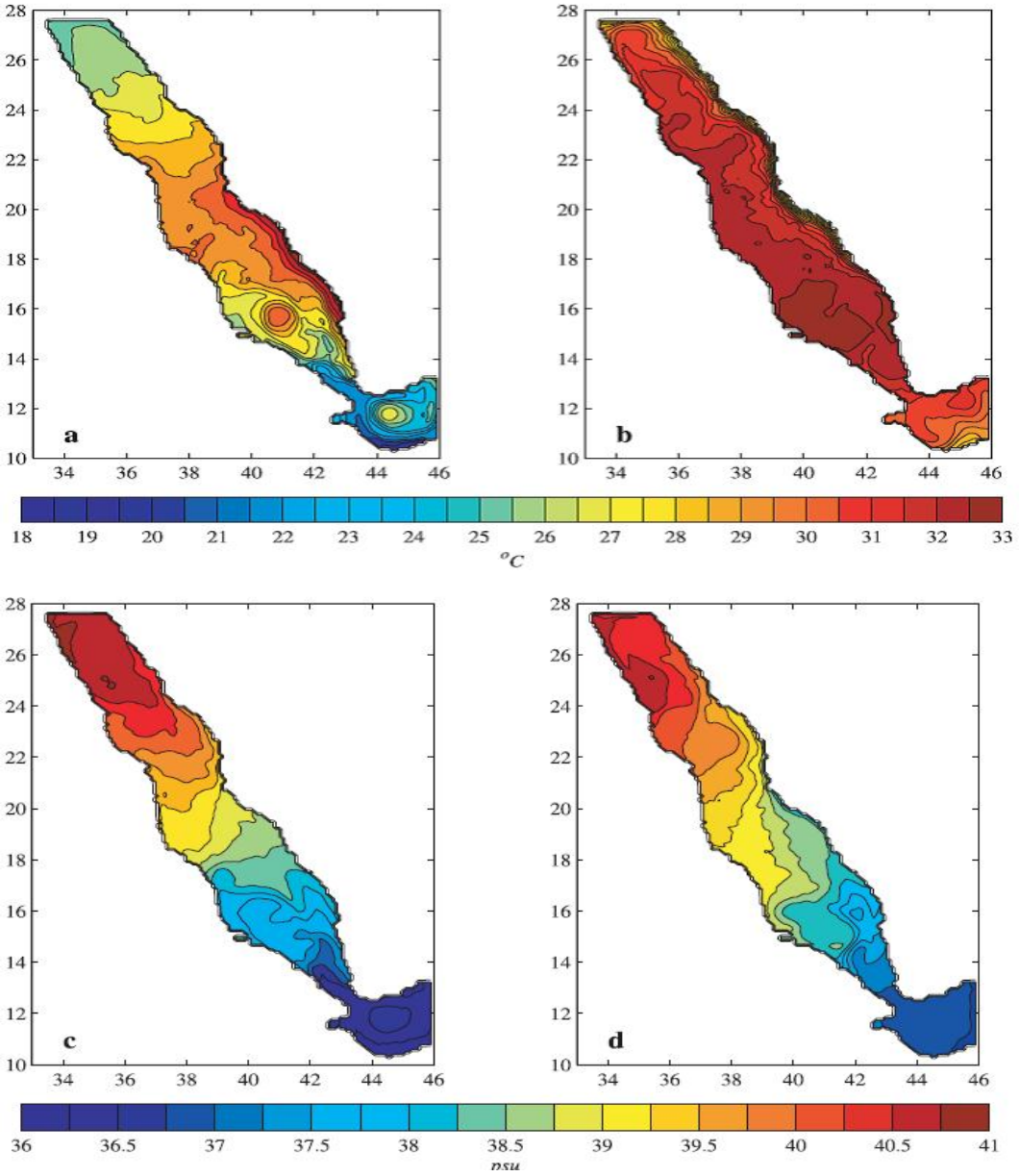

FIGURE 2.3: Seasonal sea surface temperature and salinity distribution. (a) Winter and (b) summer Sea surface temperature distribution. (c) Winter and (d) summer Sea surface salinity distribution (Sofianos and Johns, 2002).

Sofianos and Johns (2002) described the seasonal variation of SST in the Red Sea. They found that, during winter SST get their highest values at the eastern boundary of the southern and central zone due to the downwelling in the southern zone that induced by winds. While during summer the lowest values of SST are observed at the eastern boundary in the northern and middle zone of the sea due to the upwelling along the eastern boundary region. See Figure 2.3 (a and b).

Red Sea waters are classified as one of the most saline water in the world; this is due to the high evaporation, lack of runoff supply and a very little precipitation. Generally salinity at every latitude is higher in summer than in winter (Morcos,

1970). Surface salinity in the red sea increases from 36.5 psu in the southern zone to 40.5 psu in the northern zone (Neumann and McGill, 1961). This increase in salinity to the north is due to the evaporation and mixing of low saline Gulf of Aden surface inflow with the more saline deep water through turbulence (Morcos, 1970). The salinity in the northern zone ranging from (40 – 41psu) whiles in the southern zone its ranging from (36 – 37 psu). The Red Sea deep waters are warmer and more saline than any other marine basin (Halim, 1984). During summer, law salinity surface waters are found along the eastern boundary due to the inflow of cooler and fresher Gulf Of Aden Intermediate Water (GAIW) (Sofianos and Johns, 2002). See Figure 2.3 (c and d).

2.2.3 Mixed layer in the Red Sea

The Red Sea is characterized by its three layers, the mixed layer, the thermocline layer, and the deep layer. The mixed layer is formed below the surface layer. During winter the increasing in the wind stress results in deepening of the mixed layer, while during summer the mixed layer reach about 50m depth. The thermocline layer is formed below the mixed layer and extending from 50m to about 700m. Due to convective overturning of water during winter, the vertical mixing results in deepening of the thermocline layer. The third layer is the deep layer that is formed below the above layers, and it extends from 700m to the bottom of the sea with no change in temperature (Edwards and Head, 1987).

2.2.4 Red Sea circulation

The previous studies indicate that, the thermohaline and wind forces are the most important factors for controlling the Red Sea circulation. The winds alone are not the causative factor of the Red Sea circulation, the high saline Red Sea water and the formation of dense water due to the large excess of evaporation over precipitation may have controlling the circulation and movements of surface water in the Red Sea (Neumann and McGill, 1961; Phillips, 1966; Sofianos and Johns, 2002). The wind driven circulation is much weaker than that of the thermohaline, and the effect of wind is observed in the southern zone especially in the region of the water exchange between the Red Sea and the Indian Ocean at the strait of Bab el Mandeb (Sofianos and Johns, 2002). The previous studies at the strait of Bab el Mandeb express this effect of winds because there are two layer flow are formed during winter and three layer during summer. During winter a layer of surface water from the Gulf Of Aden (GASW) enters the Red Sea and flow north due to the influences of southeasterly winds, while the deep layer of the Red Sea water (RSW) flows outward to the Gulf of Aden. During summer the three layers

that formed as following: A thin layer of surface out flow waters leave the Red Sea due to the effect of north westerly winds, an intermediate layer of nutrient-rich water from the upwelling region in the Gulf Of Aden (GAIW) enters the Red Sea and flow north to substitute the out flow water, and the third layer is the bottom high salinity out flow to the Gulf Of Aden (Neumann and McGill, 1961; Phillips, 1966; Morcos, 1970). Figure 2.4 illustrates the two circulation patterns in the Bab el Mandeb during winter and summer seasons.

The mechanism of thermohaline circulation in the Red Sea was described by (Neumann and McGill, 1961; Phillips, 1966), they show that, the warm surface waters from the Gulf Of Aden enters the Red Sea through the strait of Bab el Mandeb, move northward, it cools due to the effect of winds, and became more saline because of the evaporation. The decrease in temperature (cooling) and the increase in salinity of the water leads to an increase in its density, which in turns forcing the denser water to sink in the northern zone and return to the south as a warm high-salinity subsurface water, which flows out over the shallow sill into the Gulf of Aden.

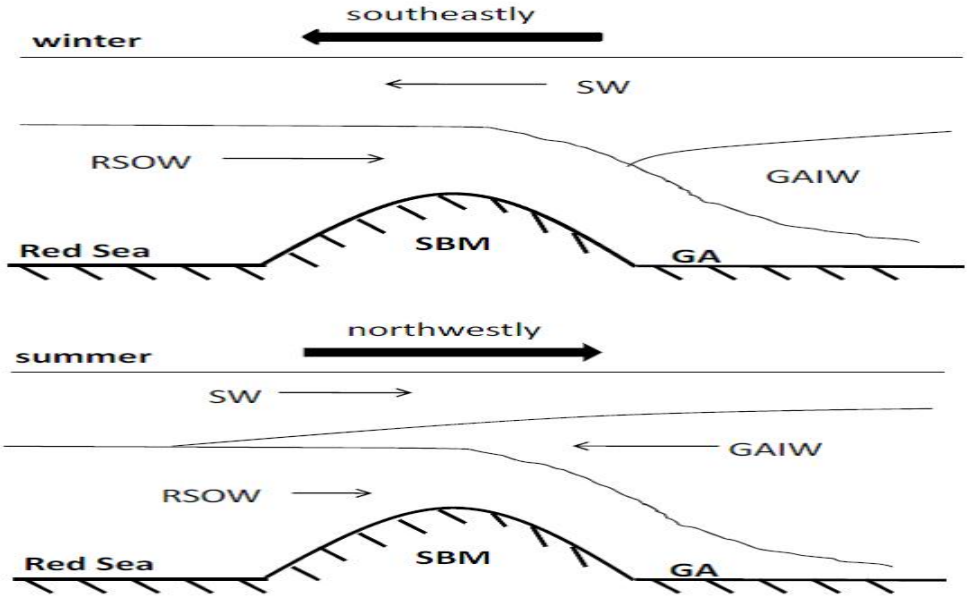

FIGURE 2.4: Sketch of the two circulation patterns in the Bab el Mandeb. Left: winter, right: Summer. SW=surface water, GAIW=Gulf of Aden intermediate water, RSOW=Red Sea Overflow Water, SBM=Strait of Bab el Mandeb, GA=Gulf of Aden (reproduced from Smeed (2004)), (Zhai, 2011).

2.3 Bio-chemical processes

2.3.1 Nutrients and primary production in the Red Sea

Red Sea surface waters are classified as oligotrophic water (clear water with low concentration of nutrients) due to the hot, dry climate and low land run-off contribute to the low productivity of the sea (Douabul and Haddad, 1970). The Red Sea deep water has a higher concentration of nutrients than the surface water, and there is a very strong pycnocline separated these two types of water, (Häse et al., 2006). The highest nutrient concentrations were observed in the southern part of the Red Sea due to the inflow of high nutrients water from the upwelling areas of the Arabian Sea and Gulf of Aden through the Bab el Mandeb strait in the south (Douabul and Haddad, 1970).

The dissolved nutrients decrease northward rapidly due to phytoplankton uptake, thus the surface nutrients are low everywhere except in the southern part of the Red Sea (Ali, 2008). The primary production in the Red Sea has its highest value in the southern part and it is low in the middle and northern regions. It's related to the distribution of nutrients, which means that the biological productivity in the Red Sea depends on the concentration of nutrients rather than the light intensity (Acker et al., 2008). Another finder support this idea is Shaikh et al. (1986) who showed that the light intensity was never been a limiting factor for the phytoplankton productivity in the Red Sea. The highest rates of production were coincided with the lowest seasonal levels of the solar radiation. Also he thought that intense solar radiation may inhibit the photosynthesis due to the low number of phytoplankton species at the mid-summer months when there is a high intensity of light.

Wind stress is central to the strength of the upwelling in the southern zone and winter cooling might have some control on the advection of nutrients to the surface and production at this region (Baars et al., 1995). In the northern part of the Red Sea the deep vertical mixing in winter is responsible for the distribution of nutrients homogenously in the mixed layer while the stratification is the factor which controlling the vertical distribution of nutrients during the summer season (Häse et al., 2006), on the other hand, subsurface nutrients are high everywhere and therefore, deepening of the mixed layer depth (e.g. by wind induced mixing, winter cooling, etc) might represent an input of additional nutrients into the mixed layer. Episodic increase in primary productivity in this region was attributed to wind induced surface currents in the Gulf of Aqaba in the northern end of the Red Sea (Iluz et al., 2009). In the central part, Shaikh et al. (1986) showed that, peaks in primary production were associated with the seasonal stratification.

2.3.2 Phytoplankton and surface chlorophyll concentration in the Red Sea

The previous studies on the Red Sea show that, during winter phytoplankton species enter the Red Sea through the inflow from the Gulf of Aden and their concentration decrease northward. They are richer in the southern zone than that in the northern zone. The central zone (zone of convergence) is classified as the poorer zone in phytoplankton species (Halim, 1984).

Acker et al. (2008) has studied the seasonal variation of monthly mean (CHL-a) for the northern zone of the Red Sea. He used satellite chlorophyll data during the period 1998–2004. He found that, the concentration of CHL-a is very low below 0.2 mg/m^3 and the highest value of CHL-a occurred on March due to convective overturning of water. The decrease in temperature in the northern part results in convective overturning of water which brings nutrients to the surface and increase the CHL-a concentration. This situation results in negative correlation between CHL-a and SST at this part of the Red Sea. He stated that, the bloom duration is very short due to the low value of CHL-a and the stratification of the water in the northern part of the Red Sea.

Chapter 3

Satellite data algorithms

Discovering the ocean from space by using satellite data became one of the most important techniques for investigating the mysteries of the ocean and for understanding of oceanography and ocean processes. In the recent years the scientists and researchers used remote sensing data to produces promising results to understand the processes in the ocean which are difficult and costly when they used ships measurements (Robinson, 2010). In the present work we used satellite ocean color data (CHL-a, SST, and PAR) and oceanographic (Wind speed) modeling (MLD) data .

3.1 Ocean color data

The ocean color remote sensing data are used to estimate the concentration of the materials those give the ocean its apparent color. In remote sensing the ocean color is defined as the magnitude and the spectrum of the light that leaving the sea water which originally come from the sun. In practice, it is the spectral radiance at the top of the atmosphere that is measured from a satellite. As shown in Figure 3.1, this consists of light reflected by the atmosphere, the sea surface, and (in very shallow water) the sea bed, as well as backscattered by seawater constituents (Robinson, 2010).

When the light enters the sea, it interacts with the constituents of the sea water. Depending on the sea water contents the light is either absorbed or scattered. The probability of scattering or absorption depends on the wavelength of the light and the material which it counters. Sea water molecules scatter the shorter wave lengths of light (blue part of the spectrum), and absorbs the longer wave lengths

(red end of the spectrum). The scattered light give the sea it's appearing color (Robinson, 2010).

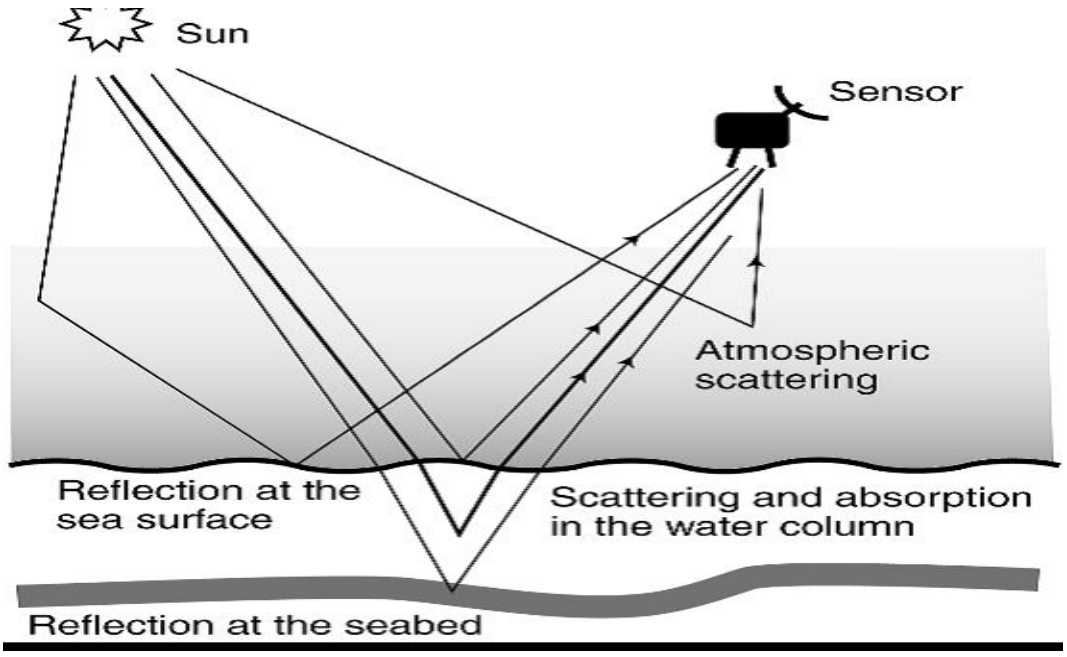

FIGURE 3.1: Factors which affect the light reaching an ocean color sensor (Robinson, 2010).

3.1.1 Chlorophyll-a Algorithm

According to the fact that phytoplankton pigments absorb energy primarily in the red and blue regions of the spectrum and reflect green light, the CHL-a pigments which is found in phytoplankton, absorbs the light strongly in 440 nm in the blue region but not in the green. The color of the ocean is determined primarily by the abundance of phytoplankton and their associated photosynthetic pigments as discussed earlier in the introduction. As the concentration of CHL-a increases, more blue light are absorbed, and more green light is scattered then, the ocean color shift from blue to green. The typical form of an algorithm to estimate the concentration of chlorophyll-a (C) is:

$$C = A\left(\frac{R_{550}}{R_{490}}\right)^{B}.$$

Where A and B are empirically derived coefficients, R_λ is reflectance (radiance coming out of the sea towards the sensor, normalized by incoming irradiance) over a spectral waveband of the sensor centered at wavelength λ. This is described as the green/blue ratio algorithm which work very well for the estimation of C in case 1 waters where the phytoplankton is the only factor that affect the color (Robinson, 2010).

3.1.2 Sea Surface Temperature (SST) algorithm

There are various methods of measuring SST at different levels of the near-surface thermal structure of the ocean. This is due to the different kinds of SST; skin SST, which is the temperature in the top few microns at the sea surface, and subskin SST, which is the temperature in a short distance (1mm) from the surface.

Skin SST are measured by thermal infrared radiometer SST while, subskin SST are measured by microwave radiometers which penetrate deeper than Infrared radiometers. The two radiometers are used for measuring the radiation temperature of the sea surface directly, because in the thermal infrared and microwave parts of the spectrum the most observed radiation is thermally emitted by the sea surface. We used data from the Advanced Very High Resolution Radiometer (AVHRR) on board of NOAA satellites, which used infrared radiometry for measuring SST (Robinson, 2010).

3.1.3 Photosynthitically Available Radiation (PAR) Algorithm

PAR is a very important factor for controlling the primary production in the ocean, and also it's represent the helping factor in the photosynthesis. The global estimates of primary production need information's about the global distribution of solar irradiance which produces by remote-sensing satellites. Solar irradiance can be calculated from the solar constant and Earth–Sun geometry for a particular time, and location on the Earth using irradiative transfer models. This model estimate the PAR under both cloud free and cloudy condition (Robinson, 2010).

The particular case for measuring PAR appear when, it is limited to the visible wavelengths of light where the absorption of light by clouds is practically zero. In this case the irradiance leaving the cloud base towards the ground is the difference between solar downward irradiance at the top of the cloud and upward irradiance leaving the cloud.

The global maps of PAR reaching the sea surface were generated daily from SeaWiFS data. The method assumes decoupling the effect of clouds on light reaching the ground from the effect of a clear atmosphere. Figure 3.2 show an example of typical global maps of PAR from an 8-days period which its smooth but still shows considerable weather dependence (Robinson, 2010).

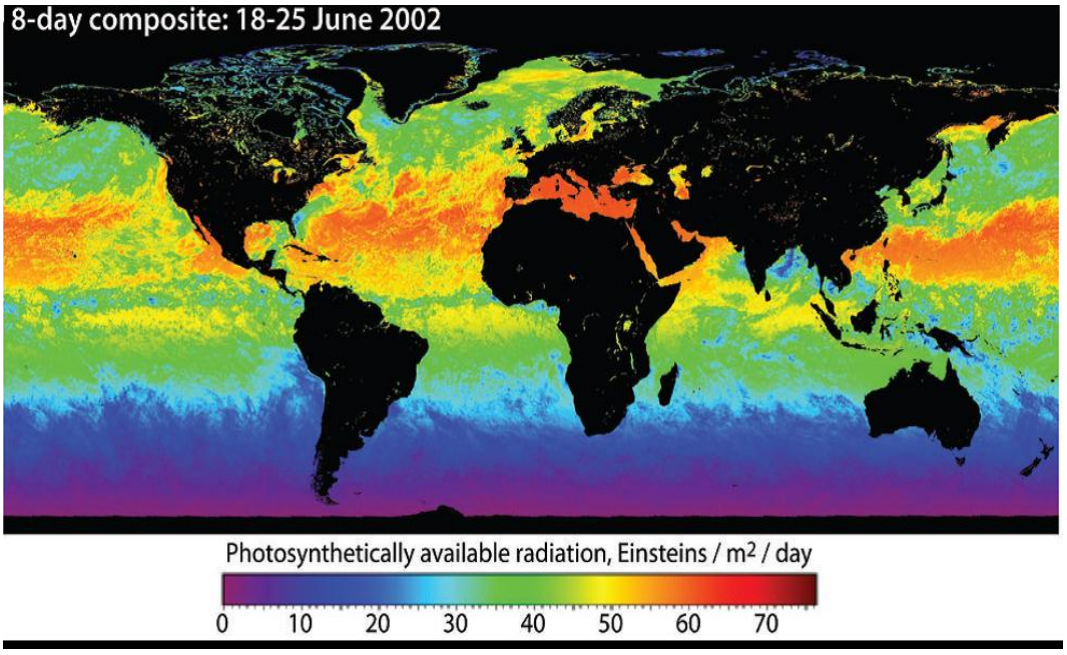

FIGURE 3.2: Examples of 8-day average PAR distributions for the period June 18–25, 2002 derived from SeaWiFS data (Robinson, 2010).

3.2 Wind data algorithm

Winds are affecting the surface water of the sea by producing small ripples, which become steeper and longer as the wind speed increase. In the recent years, ocean scientists turns to global wind forecasts of meteorological agencies, based on numerical weather prediction (NWP) models in order to study the winds over the sea surface. They used the reanalysis data which have a better quality than the remote sensing data. The National Center for Environmental Prediction (NCEP) which used in the present study is one of the widely used sources of reanalysis wind data (Robinson, 2010).

Chapter 4

Data and method

4.1 Data Sources description

The data required for the present study were obtained from the databases of the following agencies: The European Service Agency for Ocean Color data (ESA), NOAA National Oceanographic Data Center (NODC), the Ocean Color website, Global NCEP data (National Center for Environmental Prediction) NOAA Earth System Research Laboratory) and HYCOM (HYbrid Coordinate Ocean Model). The European Service Agency for Ocean Color data produces long time series of ocean color data merged from four satellite data sources, the medium resolution imaging spectrometer instrument (MERIS) aboard ENVISAT, the moderate imaging spectrometer (MODIS) on the aqua earth observing system (EOS) mission, and the sea-viewing wide field of view sensor (SeaWiFS) on board OrbView-2.

Surface Chlorophyll Concentration (CHL-a) products were derived from data obtained by ESA using medium resolution imaging spectrometer instrument (MERIS) aboard ENVISAT. It has an accuracy of (ocean color bands typical S: N = 1700) and spatial resolution of (1040m×1200m in the ocean), and (260m×300m in land and coast). The sensor provides reliable data for the Red Sea at a nominal spatial resolution of 1/24 grid (around 4.63km average bin size). The output were in binned data format stored in netCDF (Net work Common Data Form) files (Barrot et al., 2007).

Sea Surface Temperature (SST) data were received from the NODC Pathfinder Version 5.0 dataset. This dataset derives sea surface temperature product with spatial resolution of 4km from the Advanced Very High Resolution Radiometer (AVHRR) imagery. The data were stored in hierarchical data format version 4 (HDF 4).

The data were originally produced with remote sensing techniques, particularly satellite imagery. The data were averaged over 8 day's intervals for the period 1998 to 2009. Henceforth, the 8 days intervals will be referred to as weeks.

Reanalysis daily wind data used in this study were downloaded from the National Center for Environmental Prediction (NCEP) data at (NOAA Earth System Research Laboratory). They are described by Kalnay et al. (1996) and available in netCDF format.

Mixed Layer Depth (MLD) data were obtained from HYCOM (HYbrid Coordinate Ocean Model) using a Matlab code for remote access using OpenDAP protocol (obtained from personal communications with A. Korosov). For the sources of the data see Table 4.1.

TABLE 4.1: Sources and specifications of the data

Parameter	Source	Resolution		period
		Temporal	Spatial	
CHL-a[1]	ESA	8 days	1/24 km	1998-2009
SST[2]	NODC	8 days	4 km	1998-2009
PAR[3]	Ocean Color website	8 days	9 km	1998-2009
MLD[4]	HYCOM	Daily	1/12 degree	2002-2007
WIND[5]	NCEP	Daily	2.5 degree	1998-2009

[1]Barrot et al. (2007)
[2]www.nodc.noaa.gov/SatelliteData/pathfinder4km/userguide.html
[3]www.oceancolor.gsfc.nasa.gov/PRODUCTS/product_level_desc.html
[4]http://hycom.org/hycom/overview
[5]March,1996 BAMS Kalnay et al. (1996)

4.2 Data extraction and identification of different zones

The above described data (CHL a, SST, and PAR) were automatically downloaded using Wget software. They have uncompressed using (7-zip software) in order to be ready for extraction and further analysis. Special software called BEAM/VISAT has been downloaded from the Earth observational toolbox and development platform. This software has been used for viewing, analyzing and processing of remote sensing raster data. It is also used to display the data which are in a form of images file in to the computer, and to navigate on the image for retrieving data in specific geographical locations (Latitude and Longitude).

The three zones (northern, middle, and southern zones) in the Red Sea have been estimated approximately by generating JPG files with CHL a, SST, and PAR for 12 dates in one year in BEAM software. Dates were selected from different months and the color of these images has changed using color manipulation techniques (applying of the color scale). At these images an areas where the mean values and dynamics of the three parameters are similar but different from other areas were found out. Two images were printed and the borders of the three zones were approximately drawn using a pen.

4.2.1 Generation of pins

The most important step for extraction the data is the generation of pins which contains information about the (x and y axis) or (longitude and latitudes) co-ordinates. Pin is defined as a tool for extracting pixel values from raster data. 150 pins have been generated for each parameter as 50 pins for each zone, with each pin corresponding to an area of ($1km^2$). In order to generate pins for the three parameters, one satellite image with mean CHL-a values has been opened in BEAM software. The three estimated zones were compared with the drawing of approximate border in the printed image. 50 pins were placed in each zone and all pins have been exported to XML file. All pins from XML file have been imported in the pin manager of the BEAM software. In the pin manager the mean values of the parameter for each pin were added. All pins with mean values were transferred into Excel file, then we have the CHL-a and SST data for each zone.

To extract PAR data, the pins were exported into a placemark file (example of such file is `chl1_north_pins`). BEAM software cannot read this type of pins file that already generated in CHL-a and SST images. This is because, files with PAR data has no geolocation information. Excel file (`xml_converter.xls` obtained from personal communication with A.Korosov) has been used to convert it into shape of file that can easily read and opened in to PAR satellite images data. The new file was saved in a form of (`par_north_pins`, placemark). It has imported in the pin manager of the BEAM software in order to extract PAR data for the three zones.

Finally Six files of pins have been generated, two for northern zone (one for CHL a / SST and one for PAR), two for middle zone (one for CHL a / SST and one for PAR), and two for southern zone (one for CHL a / SST and one for PAR).

4.2.2 Extraction of data from satellite imagery into Excel

Data was extracted from satellite images into Excel sheet in the following steps:

1. Open satellite image in BEAM.
2. Open file with pins.
3. Import pins, add row parameter- mean, copy to clipboard.
4. Paste the pins with values of X, Y, Lat, Lon, parameter mean, etc to the upper-left most corner (Cell A1). See Figure 4.1, columns A – H.
5. Change the cell with *parameter mean*. Give it a meaningful value, e.g. '`CHL1_19980101`' in order to know from which image these values of parameter were taken. See Figure 4.1 the first cell in columns H and P.
6. Do the same with the rest images for each parameter at each zone. Each time paste pins with values X, Y, Lat, Lon, parameter mean, etc to the right of the previous one I – P. See Figure 4.1.
7. To prepare the data for averaging: In the columns J – O there is no valuable information: values are the same as in the columns A – G. For that delete these columns. See Figure 4.2.
8. Do the same with the not valuable columns for other months.
9. Automatically replace NaN values with empty cells.
10. Calculate the average value for each column automatically by inserting the averaging formula. See Figure 4.2.
11. Select cell with averaged values, plot them in order to have the seasonal dynamics of the parameter.

	A	B	C	D	E	F	G	H	I	J	K	L	M	N	O	P
1	Name	X	Y	Lon	Lat	Label	Desc	CHL1_19980101	Name	X	Y	Lon	Lat	Label	Desc	CHL1_19980108
2	pin_1	5185.5	1521.5	36.0625	26.60417	Pin 1		0.293929	pin_1	5185.5	1521.5	36.0625	26.60417	Pin 1		0.242191
3	pin_2	5180.5	1524.5	35.85417	26.47917	Pin 2		0.114448	pin_2	5180.5	1524.5	35.85417	26.47917	Pin 2		0.140572
4	pin_3	5174.5	1527.5	35.60417	26.35417	Pin 3		0.129232	pin_3	5174.5	1527.5	35.60417	26.35417	Pin 3		0.1476
5	pin_4	5164.5	1533.5	35.1875	26.10417	Pin 4		0.138531	pin_4	5164.5	1533.5	35.1875	26.10417	Pin 4		0.159721
6	pin_5	5156.5	1538.5	34.85417	25.89583	Pin 5		0.171204	pin_5	5156.5	1538.5	34.85417	25.89583	Pin 5		0.224188

FIGURE 4.1: Extraction of data into Excel.

	A	B	C	D	E	F	G	H	I	J
1	Name	X	Y	Lon	Lat	Label	Desc	CHL1_19980101	CHL1_19980108	CHL1_19980116
2	pin_1	5185.5	1521.5	36.0625	26.60417	Pin 1		0.293929	0.242191	0.311332
3	pin_2	5180.5	1524.5	35.85417	26.47917	Pin 2		0.114448	0.140572	0.132714
4	pin_3	5174.5	1527.5	35.60417	26.35417	Pin 3		0.129232	0.1476	0.134089
5	pin_4	5164.5	1533.5	35.1875	26.10417	Pin 4		0.138531	0.159721	0.314813
6	pin_5	5156.5	1538.5	34.85417	25.89583	Pin 5		0.171204	0.224188	0.205109
Average mean for the parameter								0.169469	0.182854	0.219611

FIGURE 4.2: Preparation of data for averaging.

4.2.3 DATA quality

Satellite data is not perfect and sometimes errors may be recorded by a sensor that results in low values in SST data, negative values in PAR data, and NaN values in CHL a data. Usually these bad quality pixels are located close to each other. They have been removed in order to have a high quality data. NaN and negative values were easily removed by replacing them automatically with empty cells in Excel. Weekly means and standard deviation for SST data have been calculated, the value of standard deviation tell us where are the bad values and in which week. When the weekly standard deviation is high (more than 1 °C), the corresponding week is containing suspicious values.

The weekly mean and weekly standard deviation plots have been made to assess where the bad values and what are the values cause high standard deviation. If half or most of the pins at the corresponding week are “infecte” by bad quality, all values (even those who seems OK) must be deleted. If only few pins are influenced by bad quality, only erroneous values must be deleted.

4.2.4 Mixed Layer Depth data processing

MLD data for the three zones in the Red Sea were obtained from HYCOM, daily data have been downloaded for the period 2002 to 2007. The data were separated to four columns, the first one represent the date when the data were taken, and the other three columns contains the MLD data for the three zones arranged from North, Middle to Southern zone. Columns of date and MLD data for each zone were taken in a separate excel sheet. For each row the day of year has been determined from the given date and used to determine the week number (day/8). The weekly averages of MLD for all years were calculated from daily values and

the seasonal dynamics for each zone has been plotted. Same processes have done for the other zones.

4.2.5 Winds data extraction and processing

Winds data for each zone were extracted using Matlab program (obtained from personal communication with Abidr). The program takes the geographical limits for each zone (illustrated in chapter 5 by a table) as inputs and extracts winds data for that zone. For each zone the number of pins which corresponding to the latitudes and longitudes were substituted in Matlab program to get the wind speed data. The resulting data were processed by the same way as the MLD data processed. Wind speed (U) seasonal dynamics for each zone were then plotted.

Chapter 5

Results and discussion

We first focus on the Red Sea in general (spatial dynamics) and then study seasonal dynamics in each zone in details.

The map of the three estimated zones which used in the present study is illustrated in Figure 5.1 and the geographical limits (latitudes and longitudes) for each estimated zone are shown in Table 5.1.

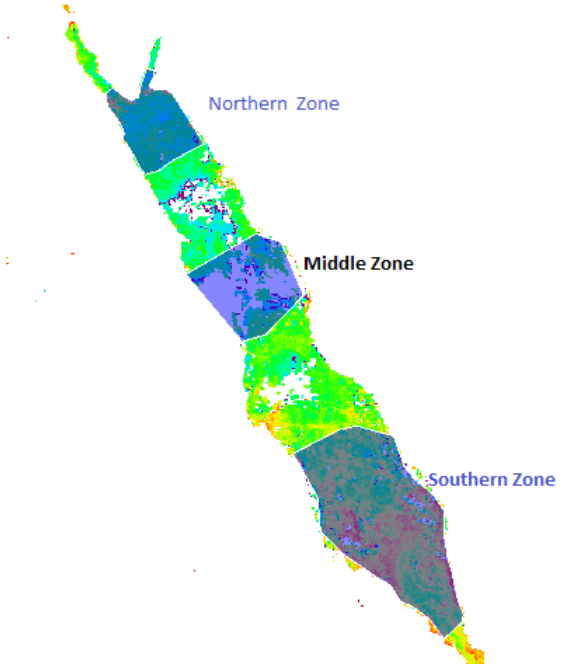

FIGURE 5.1: Map of the three estimated zones in the Red Sea (North, Middle, and South).

TABLE 5.1: The geographical limits for the three zones.

zones	Latitudes		Longitudes	
	Beginning	Ending	Beginning	Ending
Southern zone	13.47 °N	18.56 °N	38.93 °E	42.97 °E
Middle zone	21.35 °N	24.10 °N	35.85 °E	38.77 °E
Northern zone	25.85 °N	28.52 °N	33.60 °E	36.60 °E

5.1 General description of the seasonal variation of (CHL-a) in the Red Sea

Our results indicate that, during winter the mean surface chlorophyll concentration is higher in the southern zone (more than 0.4 mg/m^3) comparing to the middle (less than 0.15 mg/m^3) and northern zone (about 0.15 mg/m^3), see Figure 5.1.B. This is due to the influx of high nutrients water from the upwelling areas of the Arabian Sea and Gulf of Aden through the Bab el Mandeb strait (Ali, 2008). Also this is agree with (Koblentz-Mishke et al., 1970; Weikert, 1987), they stated that the primary production in the entire Red Sea increase from north to south according to the distribution of nutrients which comes from the Arabian Sea and Gulf of Aden.

During winter, SST has the highest value in the southern zone (31°C) and decreases through the middle (29°C) to the northern zone (27°C). Also during summer, the highest value occurs in southern zone (33°C) followed by the middle (32°C) and northern zone (30°C) see Figure 5.1.C. This is agreeing with the fact that the SST in the Red Sea increases from north to south (Acker et al., 2008).

During the summer season, the highest value of the light intensity (PAR) was observed in the northern zone (about 56 Einstein/m^2/day) comparing to the middle (55 Einstein/m^2/day) and southern zone (52 Einstein/m^2/day). While in winter season, the highest value was observed in the southern zone (44 Einstein/m^2/day) comparing to the middle (42 Einstein/m^2/day) and northern zones (40 Einstein/m^2/day). See Figure 5.1.D.

Mixed layer depth (MLD) is very shallow in the southern zone (7 m), about (15 m) in the middle and goes deeper in the northern part to a depth of (32 m) found in winter season. During summer the MLD is shallow in all three zones throughout the year Figure 5.1.E.

The strongest wind speed during summer is observed in the northern zone of the basin (4.5 m/s), while during winter the strongest winds are observed in the southern zone (4.2 m/s). The weakest wind speed is found in the zone of convergence

(central zone), (2.4 m/s) during summer and (3.4 m/s) during winter (see Figure 5.1.F).

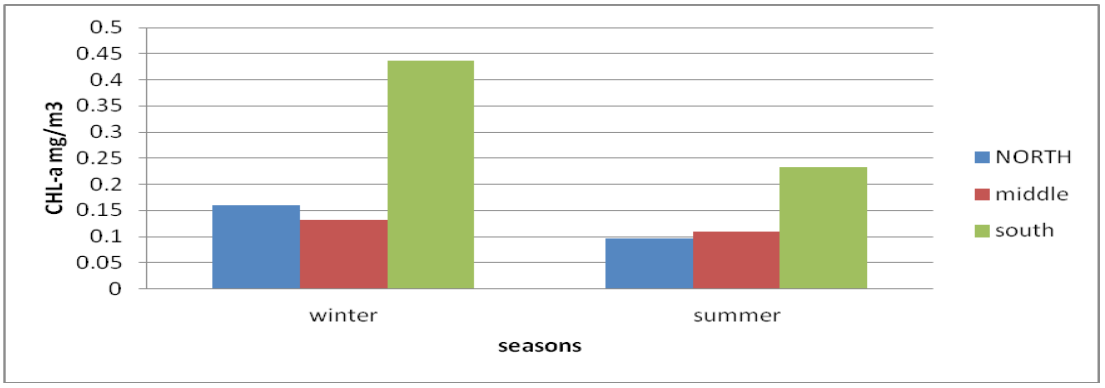

FIGURE 5.1.B: The seasonal variation of the surface chlorophyll concentration during winter and summer seasons at three zones in the Red Sea.

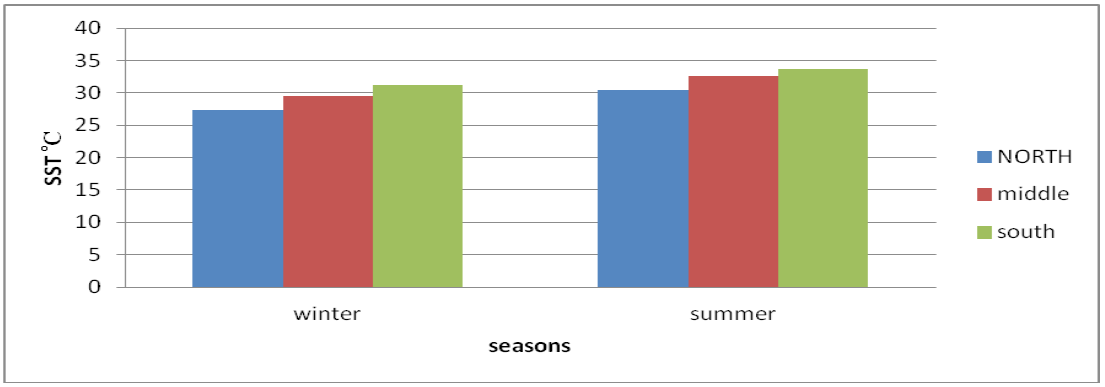

FIGURE 5.1.C: The seasonal variation of sea surface temperature during winter and summer seasons at three zones on the Red Sea.

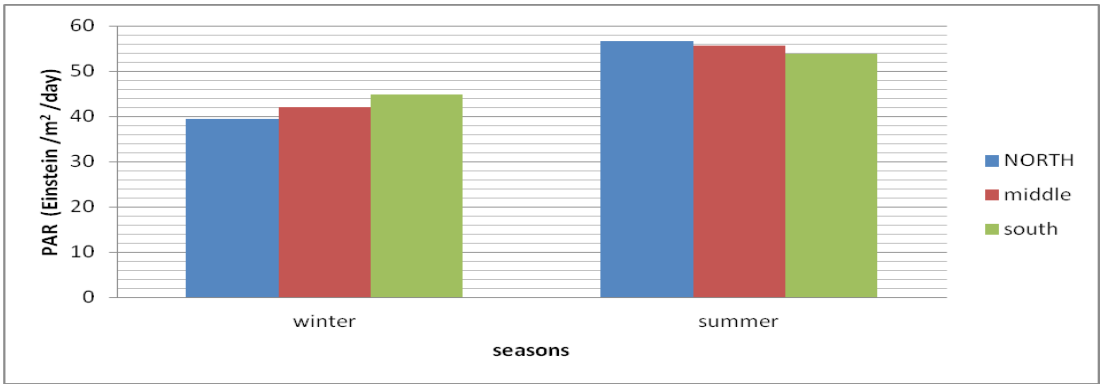

FIGURE 5.1.D: Light intensity variation through winter to summer seasons at the three zones of the Red Sea.

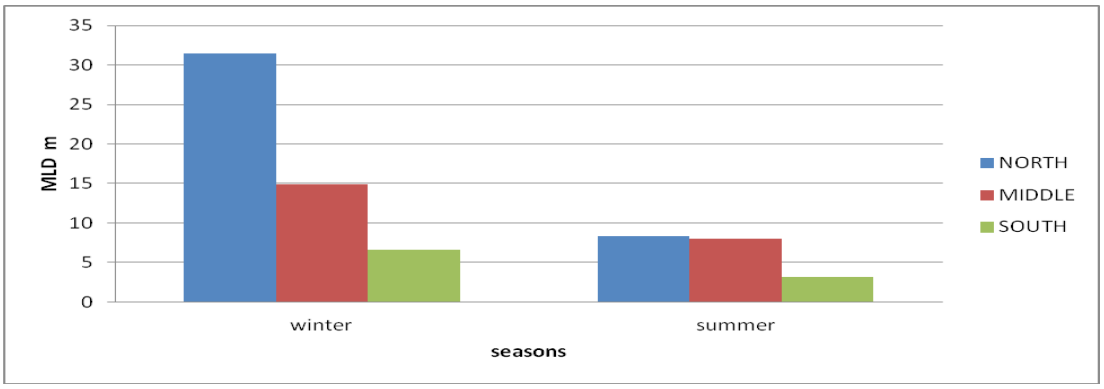

FIGURE 5.1.E: Winter to summer mixed layer depth (MLD) variability at the three zones of the Red Sea.

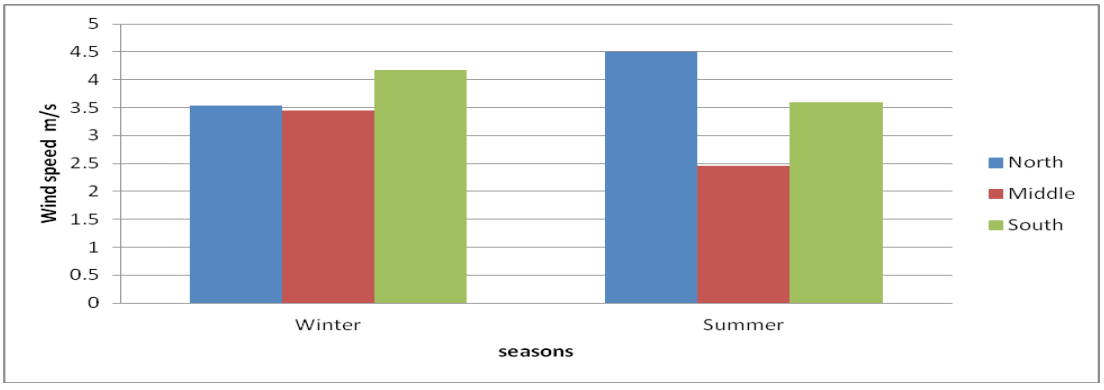

FIGURE 5.1.F: Wind speed variation through winter to summer season in the Red Sea.

5.2 Seasonal dynamics of phytoplankton bloom in the Northern Zone of the Red sea

Seasonal variation of phytoplankton bloom was detected by the (CHL-a) concentration. Weekly (CHL-a) over the period of study are very law ranging from (0.09 mg/m^3) in summer to (0.23 mg/m^3) in winter. A bloom was detected in winter when (CHL-a) starts to increase on October 15 (week 37) and ends on April 7 (week 13). The bloom gets the highest value (0.23 mg/m^3) on March 21 (week 11). On April 15 (week 14), the (CHL a) starts to decrease and continues decreasing in summer until the end of May (week 20). Then (CHL-a) becomes semi constant and continuous like that until the end of summer (Figure 5.2.A.

Figure 5.2.C shows that, SSTs are lower in winter (25 – 27°C) than in summer. Figure 5.2.D shows the seasonal variation of wind speed during winter (4 – 5 m/s) and summer (4 – 6 m/s). The MLD deepens in winter when it reach it's a maximum depth (60 m) while in summer, the MLD begins to shallow and reaches to a minimum of less than 5 m (Figure 5.2.B.

The Linear regression analysis reveals a high correlation (0.86) between CHL-a concentration and MLD, see Figure 5.2.F, negative correlation (-0.94) between CHL-a and SST same as found in (Acker et al., 2008) his results (see section 2.3.2). Also a negative correlation (-0.83) occurs between MLD and SST (see Table 5.2). This correlation indicates that, the mixed layer depth in the northern zone is controlled by the effect of the SST. According to the explanation of thermohaline circulation in the Red Sea by Neumann and McGill (1961); Phillips (1966), the decrease in SST (surface cooling) and the increase in salinity leads to an increase in density of surface water. The increase in density forces the water to sink which results in deepening of the mixed layer depth at this zone.

The minimum value of SST and the maximum value of MLD occur during the same short period as the highest CHL-a concentration are observed in March (compare Figures 5.2.A, 5.2.B and 5.2.C).

Relatively high winds (4 – 5 m/s), low SST (25 – 27°C) and deep mixed layer (40 – 60 m) result in strong mixing of surface and deep waters and high flux of nutrients from the bottom. This result in winter phytoplankton bloom in the northern zone when CHL-a reaches about 0.23 mg/m^3 on March 21. This is agreeing with Acker et al. (2008) who show that, the elevated of CHL-a in March is related to the convective overturning of water. Another finder supports this explanation is what Häse et al. (2006) showed about the distribution of nutrients on the mixed layer at the northern part of the Red Sea which is a result of deep vertical mixing in winter.

PAR is rather high throughout the year ranging from 30 Einstein/m^2 in winter to 60 Einstein/m^2 in summer. However our data show negative correlation between (CHL-a) and (PAR). By comparing Figures 5.2.A and 5.2.E we found that, during winter when the light intensity is low, the (CHL-a) is high. This means that, light is not the limiting factor for phytoplankton growth, so the limiting factor is the nutrients. Another finder support this results is Shaikh et al. (1986) who stated that, the light is not the limiting factor for the primary production in the Red Sea. Our results also agree with Acker et al. (2008) who showed that, the biological productivity of surface waters in the Red Sea is related to the nutrients concentration. By comparing the seasonal dynamics of SST and PAR at each zone we found that, the growth rate of SST depends on that of PAR (compare Figures 5.2.C and 5.2.E). We will not talk about the analysis of PAR data on the other zones.

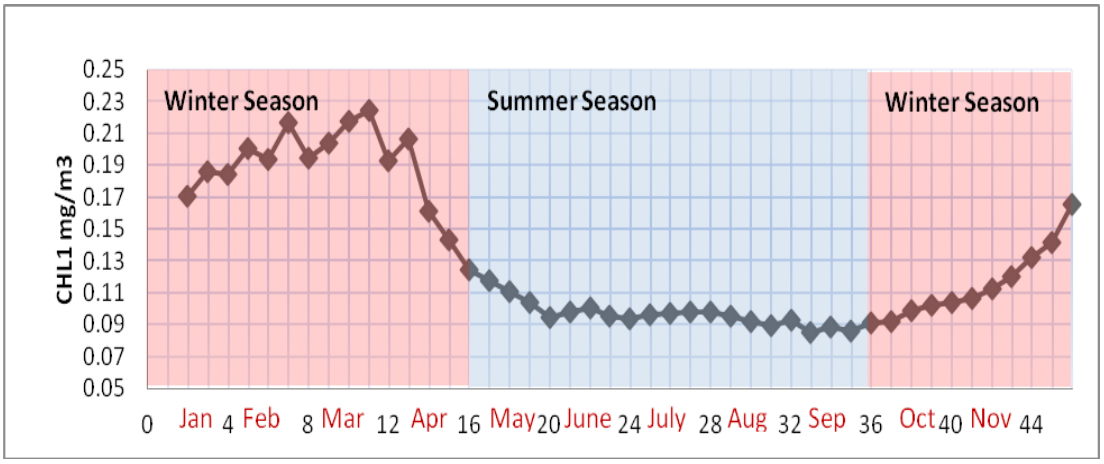

FIGURE 5.2.A: The seasonal variation of surface chlorophyll concentration (CHL-a) in the northern zone of the Red Sea.

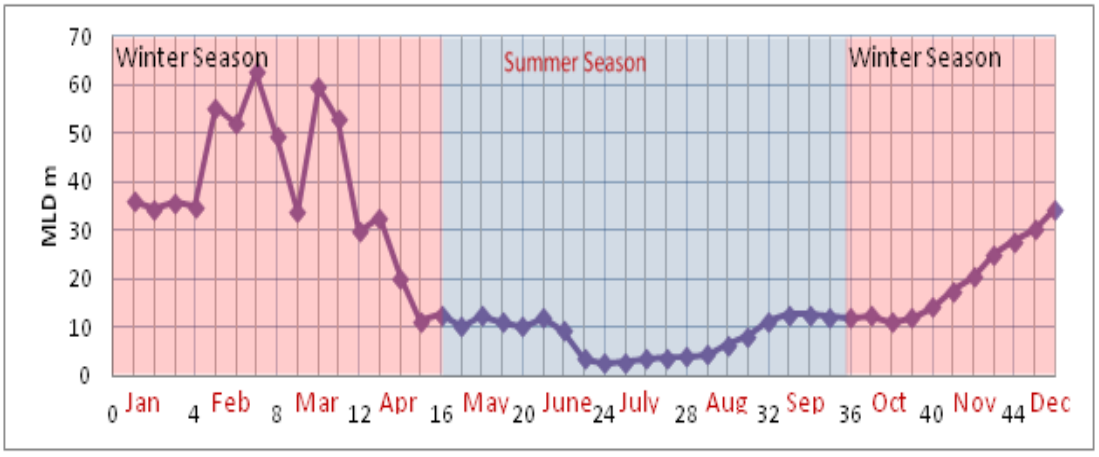

FIGURE 5.2.B: The seasonal variation of mixed layer depth (MLD) in the northern zone of the Red Sea.

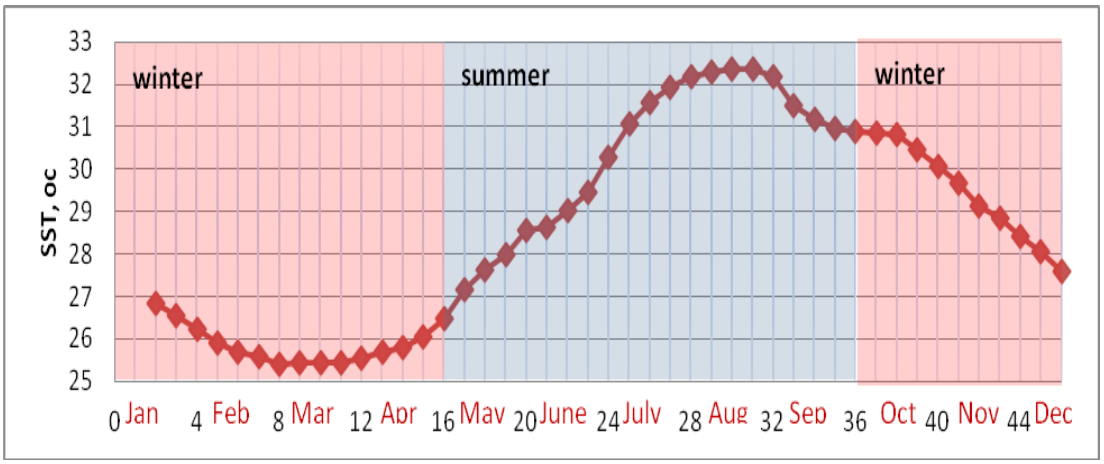

FIGURE 5.2.C: The seasonal variation of sea surface temperature (SST) in the northern zone of the Red Sea.

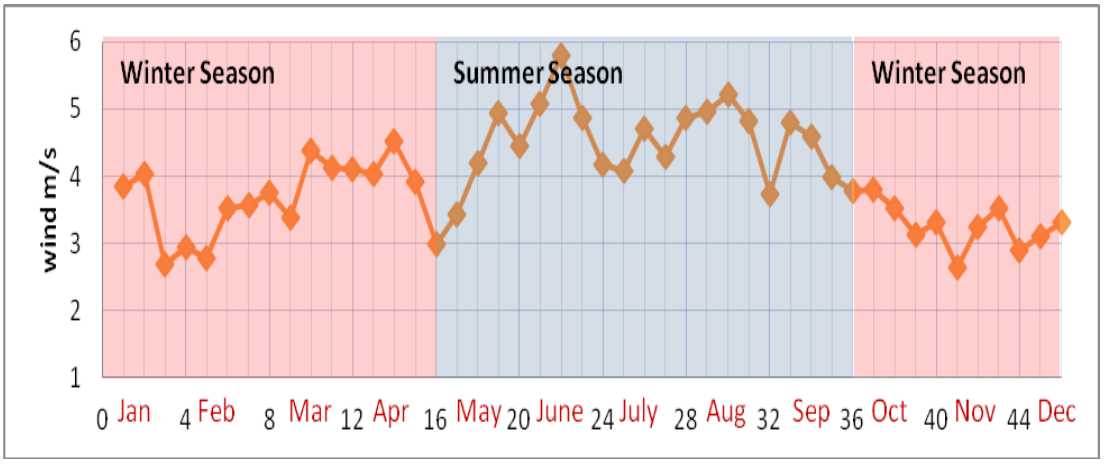

FIGURE 5.2.D: The seasonal variation of the wind speed in the northern zone of the Red Sea.

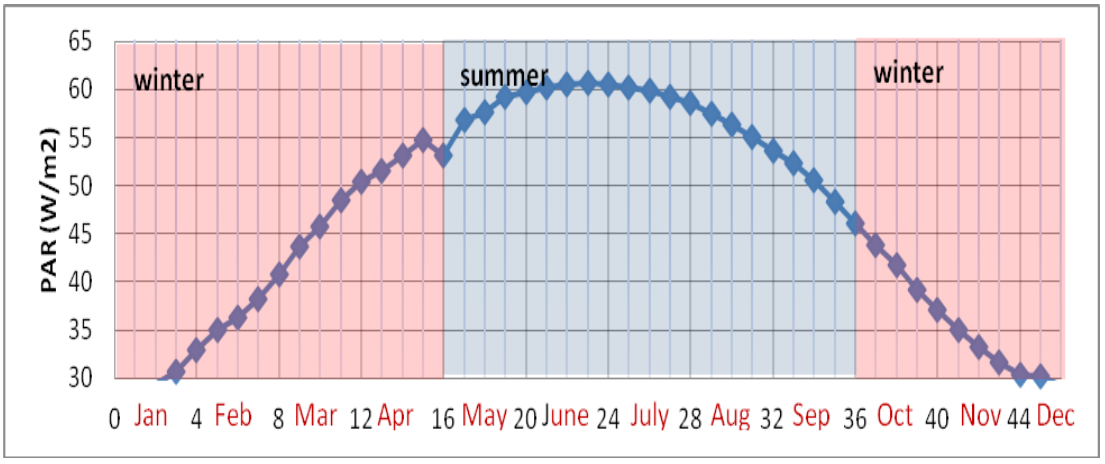

FIGURE 5.2.E: The seasonal variation of PAR in the northern zone of the Red Sea.

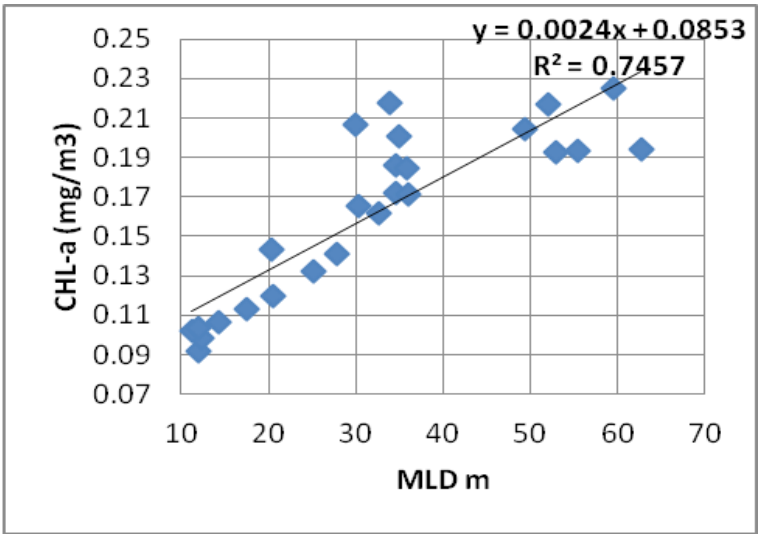

FIGURE 5.2.F: Correlation between mixed layer depth and surface chlorophyll concentration in the northern zone of the Red Sea.

TABLE 5.2: Represents the correlation between CHL-a and the parameters which influence the bloom in the northern zone of the Red Sea.

Parameter	Correlation (r)
CHL-a vs MLD	0.86
CHL-a vs Wind speed	0.17
CHL-a vs SST	-0.94
MLD vs SST	-0.83
CHL-a vs PAR	-0.47

5.3 seasonal dynamics of phytoplankton bloom in the Middle Zone of the Red sea

At this zone there is a winter bloom starts early in winter when the surface chlorophyll concentrations starts to increase on October 15 (week 37), ends on January 21 (week 3). The bloom gets its highest value (0.17 mg/m^3) at the same time when it's ending on January 21 (week 3) Figure 5.3.A. Figure 5.3.B shows that, the MLD is deeper in winter (reach about 25 m) than in summer. The bloom starts on October 15 (week 37) at the same time when winds become stronger, compare Figures 5.3.A and 5.3.D.

The correlation analysis shows positive correlations between (CHL-a) and two parameters, (0.84) between (CHL-a) and (MLD) and (0.54) between wind speed and (CHL-a) as shown in Figures 5.3.E and 5.3.F. This indicates that, the MLD and wind speed (U) may have the maximum effect on the seasonal variation of chlorophyll and the bloom in this region.

As described earlier the middle Red Sea is the zone of convergence which results in downwelling of water. The downwelling may cause the deepening of the mixed layer depth in the central zone, increase the mixing of nutrients to the surface and produce the bloom in winter. Any increase in wind speed lead to increase the nutrients by cooling the surface and deepening the mixed layer. The negative correlation between wind speed and SST support that and this is agreeing with Kahru et al. (2010) who found the correlation between winds and ocean chlorophyll in the tropical ocean.

Unlike the northern part, in winter the winds in the central part are low (3 – 4 m/s), SST is high (29 – 30°C) and, as a consequence, mixed layer is shallow (20 – 25 m). That results in weaker mixing of surface and deep waters and weak flux of nutrients from the bottom. As a result, the phytoplankton bloom in the central part is much less pronounced (CHL-a reaches only 0.17 mg/m^3).

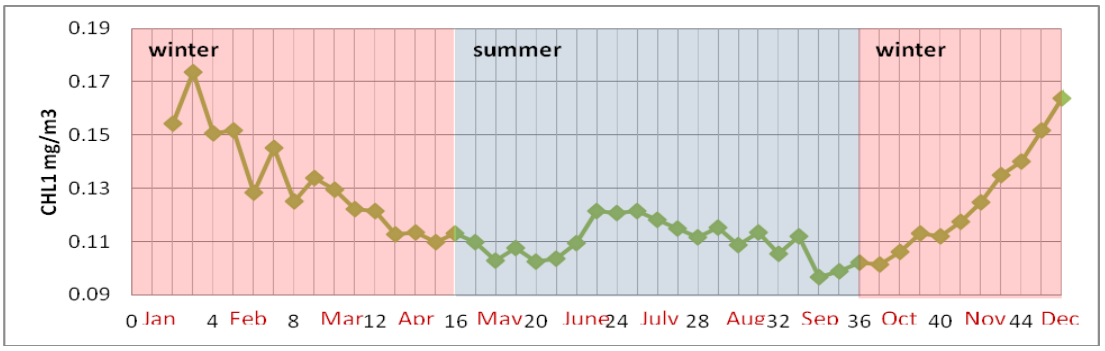

FIGURE 5.3.A: The seasonal variation of surface chlorophyll concentration (CHL-a) in the middle zone of the Red Sea.

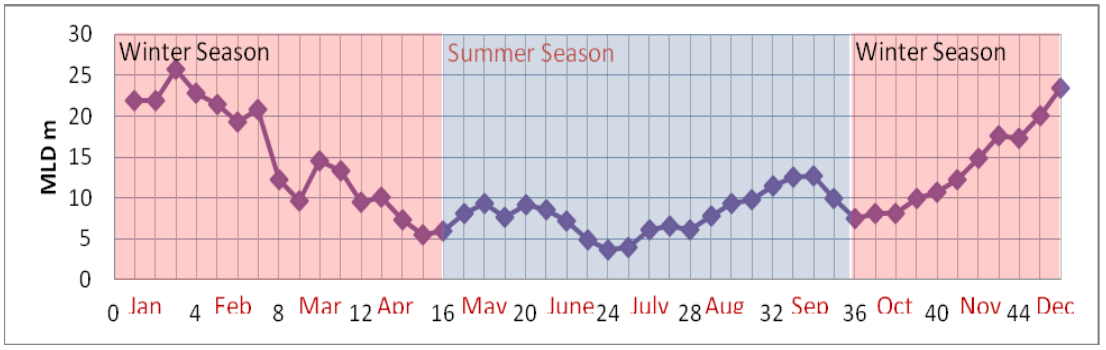

FIGURE 5.3.B: The seasonal variation of mixed layer depth (MLD) in the middle zone of the Rea Sea.

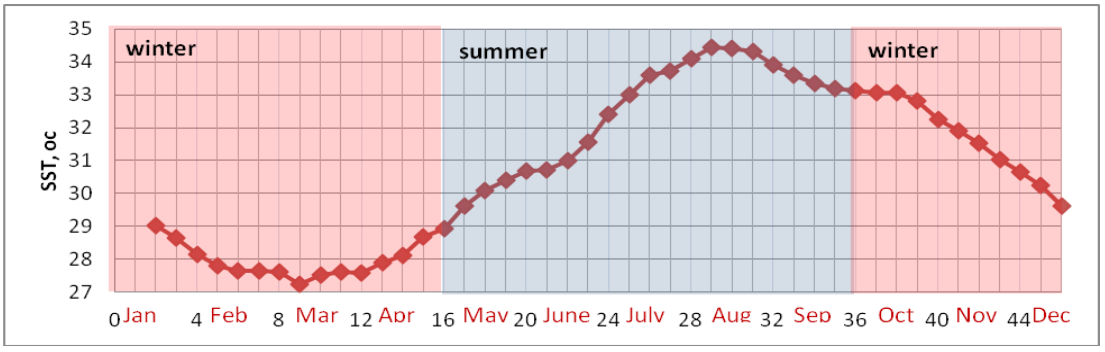

FIGURE 5.3.C: The seasonal variation of sea surface temperature (SST) in the middle zone of the Red Sea.

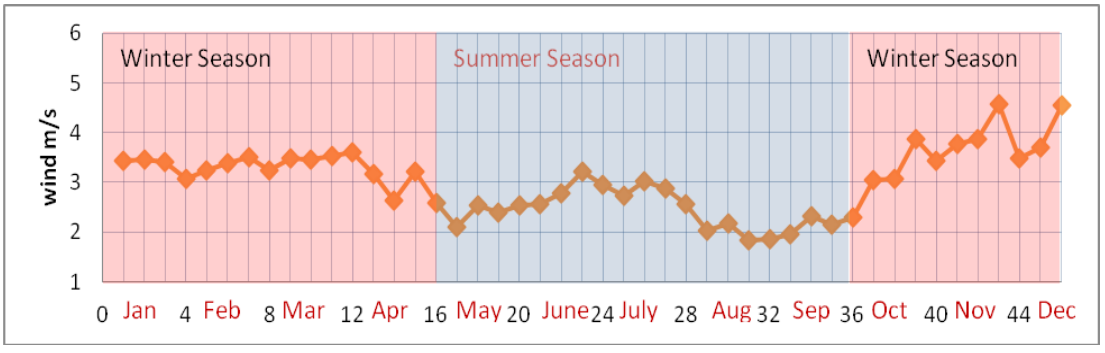

FIGURE 5.3.D: The seasonal variation of the wind speed in the middle zone of the Red Sea.

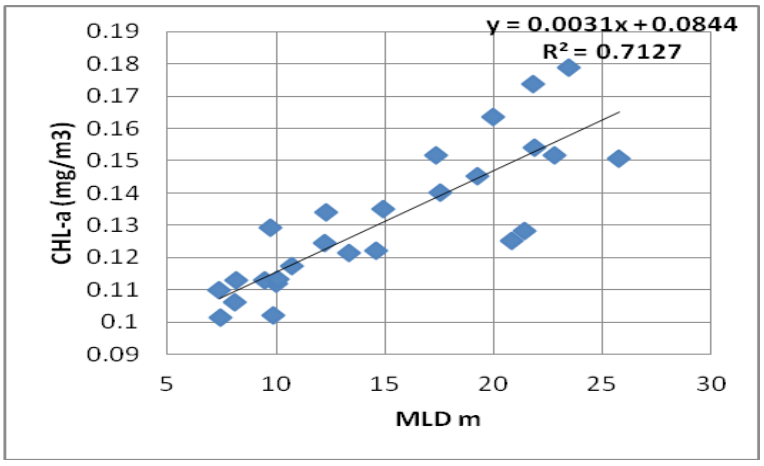

FIGURE 5.3.E: The correlation between the surface chlorophyll (CHL-a) and the mixed layer depth (MLD) in the middle zone of the Red Sea.

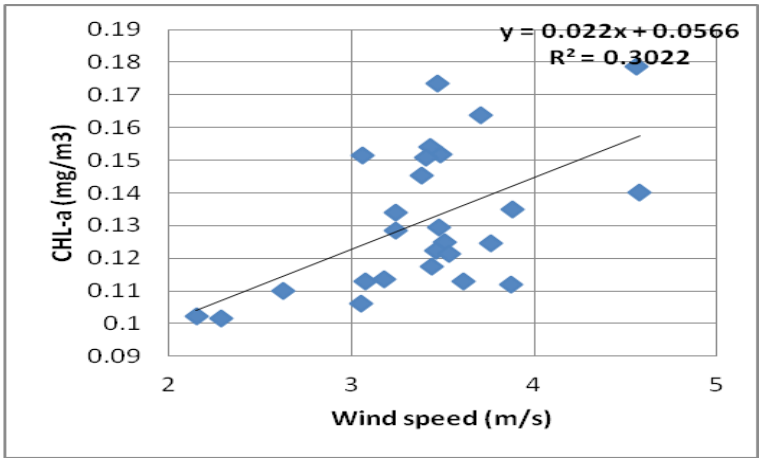

FIGURE 5.3.F: Correlation between wind speed and surface chlorophyll concentration in the northern zone of the Red Sea.

TABLE 5.3: correlation between CHL-a and the other parameters.

Parameters	Correlation
CHL-a vs MLD	0.84
CHL-a vs Wind speed	0.54
CHL-a vs SST	-0.42
SST vs Wind speed	-0.20

5.4 seasonal dynamics of phytoplankton bloom in the Southern Zone of the Red sea

At this zone the bloom starts early at the end of summer on August 21 (week 31), ends on January 15 (week 2), and getting its highest value (0.62 mg/m^3) on

December 7 (week 45). On February 7 (week 5) the concentration of chlorophyll-a starts a dramatically decrease until March 15 (week 10) as shown in (Figure 5.4.A).

In the southern zone of the Red Sea the surface layer is strongly affected by the inflowing of Gulf Of Aden Intermediate Water (GAIW) at the end of summer. Our results indicate that the bloom is starting early in summer at the same time when the high nutrients Gulf Of Aden Intermediate Water (GAIW) inflow to the Red Sea. Although there is a very strong correlation (0.86) between the (CHL-a) and MLD as shown in Figure 5.4.B, but the main factor that controlling the phytoplankton bloom in the southern zone is the advection of nutrient-rich waters from the Arabian Sea.

The interesting result of is that, the bloom in the south is much earlier than in the middle and north. This earlier bloom in the southern part may be due to winds. Winds start to blow stronger in the southern part only from week 37 and it becomes very weak on week 29, see Figure 5.4.D. That's the time when north wind stops to blow and weak south wind starts. After some time south wind becomes stronger. Probably the mechanism is the following: There is always a current from the Arabian Sea into the Red Sea due to the convective mixing (fresh warm waters come near surface from south to north, become saline and cold in the north, sink in the north, return back from north to south near bottom, flash back into the Arabian Sea). The north wind blocks penetration of nutrient rich waters from the Bab el Mandeb near the surface and warm fresh waters submerge to some depth (as in Figure 2.4). When north wind becomes weak (on week 29) surface currents from south become stronger and bring more nutrients near the surface. And only after that, south wind become stronger and intensifies advection even more. Then the bloom starts on week 31 as shown in Figure 5.4.A.

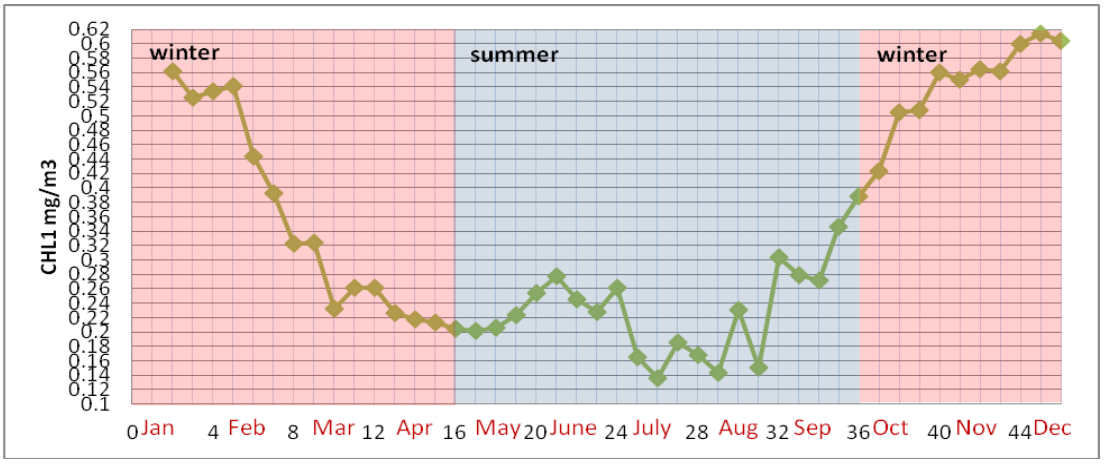

FIGURE 5.4.A: The seasonal variation of surface chlorophyll concentration (CHL-a) in the southern zone of the Red Sea.

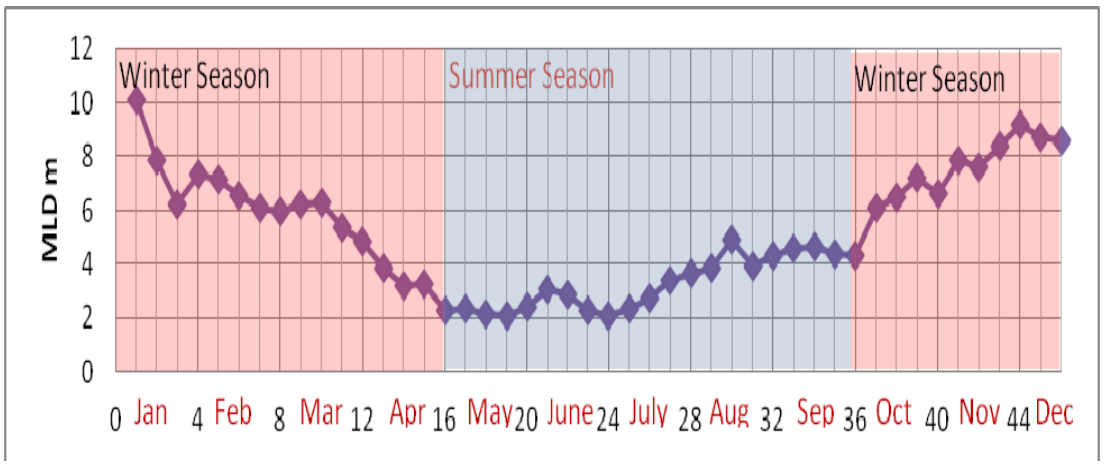

FIGURE 5.4.B: The seasonal variation of mixed layer depth (MLD) in the southern zone of the Red Sea.

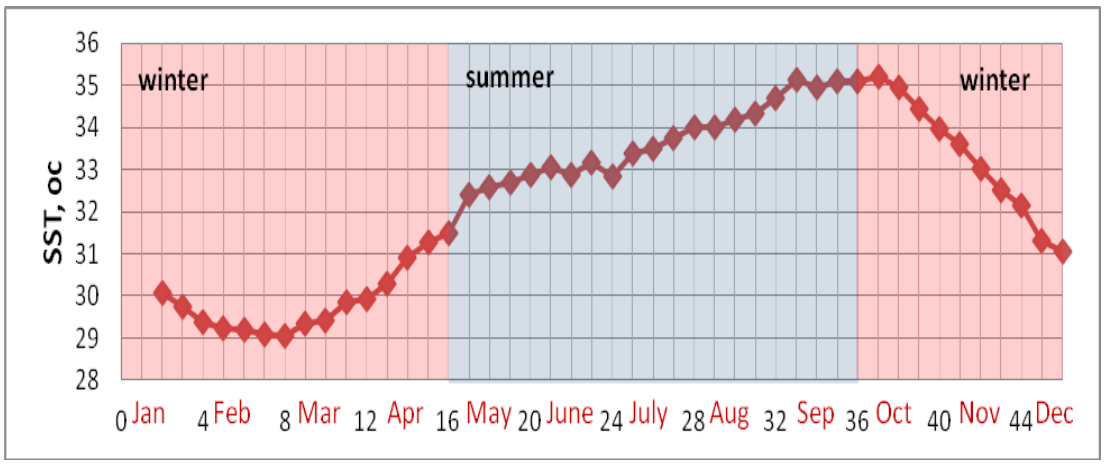

FIGURE 5.4.C: The seasonal variation of sea surface temperature (SST) in the southern zone of the Red Sea.

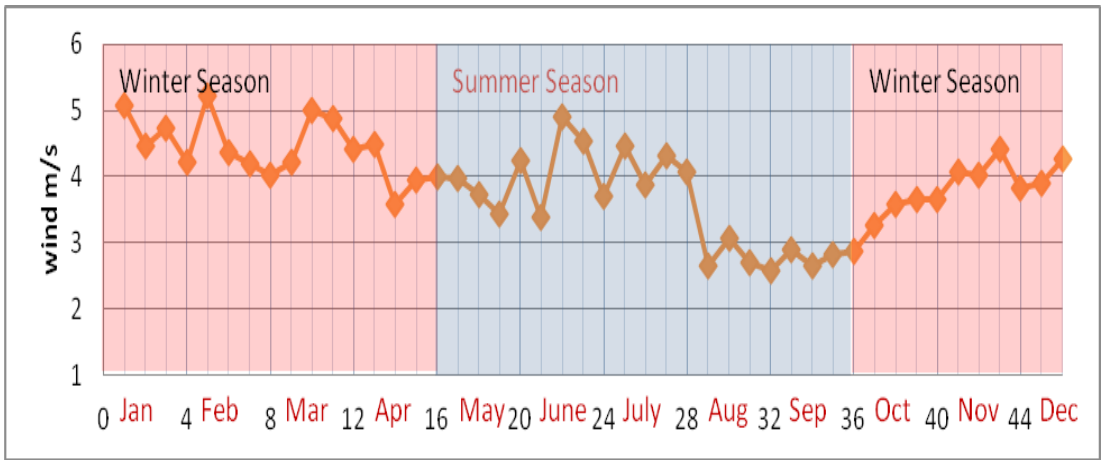

FIGURE 5.4.D: The seasonal variation of the wind speed in the southern zone of the Red Sea.

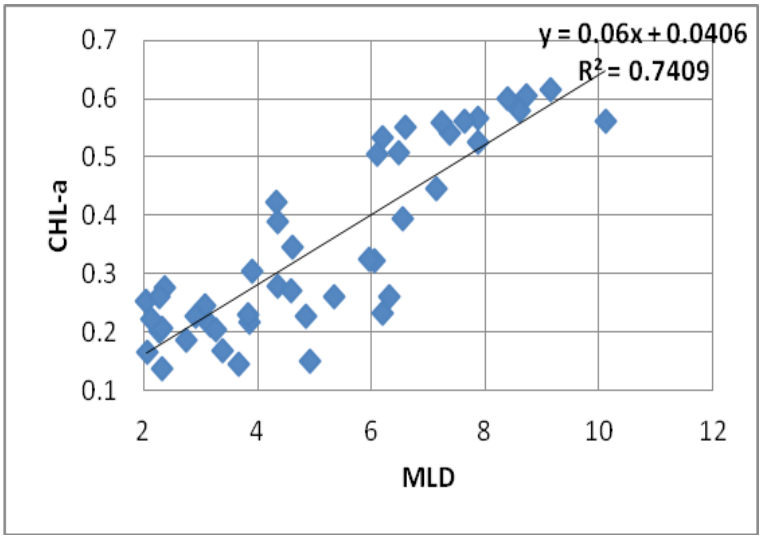

FIGURE 5.4.E: The correlation between surface chlorophyll (CHL-a) and mixed layer depth (MLD) at the southern zone of the Red Sea.

TABLE 5.4: Correlation between CHL-a and parameters in the southern part of the Red Sea.

Parameters	Correlation
CHL-a vs MLD	0.86
CHL-a vs Wind speed	-0.73
CHL-a vs SST	-0.21

Chapter 6

Conclusion

The results of this thesis can be summarized in the following points:

- We used satellite, modeling and oceanographic data for quantifying CHL-a variations and determining the controlling factors which seem to have the maximum effect in the phytoplankton bloom at three zones in the Red Sea.
- Weekly climatology of the following parameters was built from decadal observations: Surface chlorophyll concentration (CHL-a), Sea Surface Temperature (SST), Photosynthetically Available Radiation (PAR), Mixed Layer Depth (MLD), and wind speed (U).
- Mechanisms of the winter phytoplankton bloom were studied and the main factors were identified. In the northern and middle zone, the bloom is observed in winter at October 15 (week 37). The controlling factor for the bloom in the northern zone is the deepening of MLD due to convective overturning of water. While the MLD and the wind speed (U) are the most important factors in the middle zone. In the southern zone, the bloom is observed earlier at the end of summer (August 21, week 31), and the main factor is the advection of nutrient-rich waters from the Arbian Sea through Bab el Mandeb.
- In the northern zone winds are stronger and mixed layer is deeper than in the middle zone. In the southern zone winds mixing is less important but advection of nutrients is more important.
- Very interesting observation is that, the bloom in the southern zone starts 5 weeks earlier than in middle and northern zone (August 15, week 31) as shown in (Figure 5.4.A). This is probably due to the winds because the strong north wind in summer acts as a barrier for penetration of nutrient rich

waters from the Bab el Mandeb. Warm fresh waters sink to some depth as shown in (Figure 2.4). On august 7 (week 29), north wind becomes weak and surface currents from south become stronger and bring more nutrients near the surface. And only after that south wind become stronger and intensifies advection even more. Thus, different factors control not only intensity of phytoplankton bloom but also timing.

Bibliography

Acker, J., Leptoukh, G., Shen, S., Zhu, T., and Kempler, S. (2008). Remotely-sensed chlorophyll-a observations of the northern Red Sea indicate seasonal variability and influence of coastal reefs. *Journal of Marine Systems*, **69**(3):pp. 191–204.

Ali, E.B. (2008). *The Inorganic Carbon Cycle in the Red Sea*. Master's thesis, University of Bergen, Geophysical Institute.

Alvain, S., Loisel, H., and Duforêt-Gaurier, L. (2010). Observation of ocean colour beyond chlorophyll-a: From particulate organic carbon content and size distribution to phytoplankton functional groups. In: Morales, J., Stuart, V., Platt, T., and Sathyendranath, S. (eds.), *Handbook of Satellite Remote Sensing Image Interpretation: Applications for Marine Living Resources Conservation and Management*, EU PRESPO and IOCCG, Dartmouth, Canada. (pp. 65–77).

Baars, M.A., Schalk, P.H., and Veldhuis, M.J.W. (1995). Seasonal fluctuations in plankton biomass and productivity in the ecosystems of the Somali Current, Gulf of Aden, and Southern Red Sea. In: Sherman, K., Okemwa, E.N., and Ntiba, M.J. (eds.), *Large Marine Ecosystems of the Indian Ocean: Assessment, Sustainability and Management*. Blackwell Science, Oxford, UK, volume 211, (pp. 143–174).

Barrot, G., Mangin, A., and Pinnock, S. (2007). *Global Ocean Colour for Carbon Cycle Research, Product User Guide*. Reference: GC-UM-ACR-PUG-01, ACRI-ST/LOV, UoP, NIVA, BC, DLR, ICESS consortium. ESA's European Space Research INstitute, Via Galileo Galilei Casella Postale 64 00044 Frascati (RM), Italy.

Cloern, J.E. (2001). Our evolving conceptual model of the coastal eutrophication problem. *Marine Ecology Progress Series*, **210**(223):pp. 223–253.

Douabul, A. and Haddad, A. (1970). The Red Sea and Yemen's Red Sea environments. In: Douabul, A., Rouphael, T.S., and Marchant, R. (eds.), *Hassell and Assoc.*, AMSAT and UNOPS. (pp. 1–16).

Edwards, A.J. and Head, S.M. (1987). *Red Sea*, volume 7. Pergamon Press.

Halim, Y. (1984). Plankton of the Red Sea and the Arabian Gulf. *Deep Sea Research Part A. Oceanographic Research Papers*, **31**(6):pp. 969–982.

Häse, C., Al-Qutob, M., Dubinsky, Z., Ibrahim, E.A., Lazar, B., Stambler, N., and Tilzer, M.M. (2006). A system in balance? – Implications of deep vertical mixing for the nitrogen budget in the northern Red Sea, including the Gulf of Aqaba (Eilat). *Biogeosciences Discussions*, **3**(2):pp. 383–408.

Iluz, D., Dishon, G., Capuzzo, E., Meeder, E., Astoreca, R., Montecino, V., Znachor, P., Ediger, D., and Marra, J. (2009). Short-term variability in primary productivity during a wind-driven diatom bloom in the Gulf of Eilat (Aqaba). *Aquatic Microbial Ecology*, **56**(2–3):pp. 205–215.

Jiang, H., Farrar, J.T., Beardsley, R.C., Chen, R., and Chen, C. (2009). Zonal surface wind jets across the red sea due to mountain gap forcing along both sides of the red sea. *Geophysical Research Letters*, **36**(L19605):pp. 1–6.

Kahru, M., Gille, S.T., Murtugudde, R., Strutton, P.G., Manzano-Sarabia, M., Wang, H., and Mitchell, B.G. (2010). Global correlations between winds and ocean chlorophyll. *Journal of Geophysical Research*, **115**(C12040):pp. 1–11.

Kalnay, E., Kanamitsu, M., Kistler, R., Collins, W., Deaven, D., Gandin, L., Iredell, M., Sana, S., White, G., and Woollen, J. (1996). The NCEP/NCAR 40-year reanalysis project. *Bulletin of the American Meteorological Society*, **77**(3):pp. 437–471.

Koblentz-Mishke, O.J., Volkovinsky, V.V., and Kabanova, J.G. (1970). Plankton primary production of the world ocean. In: Wooster, W.S. (ed.), *Scientific Exploration of the South Pacific*, National Academy of Sciences, Washington D.C., USA. (pp. 183–193).

Li, H.P., Gong, G.C., and Hsiung, T.M. (2002). Phytoplankton pigment analysis by HPLC and its application in algal community investigations. *Botanical Bulletin of Academia Sinica*, **43**:pp. 283–290.

Liebig, J. and Playfair, B.L.P. (1845). *Chemistry in its Application to Agriculture and Physiology*. J.M. Campbell.

Lindell, D. and Post, A.F. (1995). Ultraphytoplankton succession is triggered by deep winter mixing in the Gulf of Aqaba (Eilat), Red Sea. *Limnology and Oceanography*, **40**(6):pp. 1130–1141.

Mackey, K.R.M., Rivlin, T., Grossman, A.R., Post, A.F., and Paytan, A. (2009). Picophytoplankton responses to changing nutrient and light regimes during a bloom. *Marine Biology*, **156**(8):pp. 1531–1546.

Mann, K.H. and Lazier, J.R.N. (2006). *Dynamics of Marine Ecosystems: Biological-Physical Interactions in the Oceans*. Wiley-Blackwell.

Morcos, S.A. (1970). Physical and chemical oceanography of the Red Sea. *Oceanography and Marine Biology: An annual review*, **8**(8):pp. 73–202.

Moses, W.J., Gitelson, A.A., Berdnikov, S., and Povazhnyy, V. (2009). Estimation of chlorophyll-a concentration in case II waters using MODIS and MERIS data-successes and challenges. *Environmental Research Letters*, **4**(045005):pp. 1–8.

Neumann, A.C. and McGill, D.A. (1961). Circulation of the Red Sea in early summer. *Deep Sea Research (1953)*, **8**(3):pp. 223–235.

Patzert, W.C. (1974). Wind-induced reversal in Red Sea circulation. In: *Deep Sea Research and Oceanographic Abstracts*. Elsevier, volume 21, (pp. 109–121).

Pedgley, D.E. (1974). An outline of the weather and climate of the Red Sea. *ĹOceanographie Physique de la Mer Rouge*:pp. 9–27.

Phillips, O.M. (1966). On turbulent convection currents and the circulation of the Red Sea. In: *Deep Sea Research and Oceanographic Abstracts*. Elsevier, volume 13, (pp. 1149–1160).

Robinson, I.S. (2010). *Understanding the Oceans from Space: The Unique Applications of Satellite Oceanography*. Springer Verlag.

Sarmiento, J.L. and Gruber, N. (2006). *Ocean Biogeochemical Dynamics*. Cambridge University Press.

Sarmiento, J.L., Slater, R., Barber, R., Bopp, L., Doney, S.C., Hirst, AC, Kleypas, J., Matear, R., Mikolajewicz, U., and Monfray, P. (2004). Response of ocean ecosystems to climate warming. *Global Biogeochemical Cycles*, **18**(3):pp. 3001–3023.

Shaikh, E.A., Roff, J.C., and Dowidar, N.M. (1986). Phytoplankton ecology and production in the Red Sea off Jiddah, Saudi Arabia. *Marine Biology*, **92**(3):pp. 405–416.

Smeed, D.A. (2004). Exchange through the Bab el Mandab. *Deep Sea Research Part II: Topical Studies in Oceanography*, **51**(4):pp. 455–474.

Sofianos, S.S. and Johns, W.E. (2002). An Oceanic General Circulation Model (OGCM) investigation of the Red Sea circulation, 1. Exchange between the Red Sea and the Indian Ocean. *Journal of geophysical research*, **107**(C11):pp. 3196–3206.

Weikert, H. (1987). Plankton and the pelagic environment. *Red Sea, Pergamon Press, Oxford*:pp. 90–111.

Zhai, P. (2011). *The Response of the Red Sea to a Strong Wind Jet Near the Tokar Gap in Summer*. Master's thesis, Massachusetts Institute of Technology and Woods Hole Oceanographic Institution.